Laboratory investigation of overtopping at a sloping structure with permeable shingle foreshore

M. Salauddin[1*] and J. M. Pearson[1]

[1*]School of Engineering, University of Warwick, Coventry, CV47AL, UK

Abstract

The vast majority of overtopping data applied in EurOtop (2018) has been made from small-scale measurements with impermeable foreshore slopes. This article describes a comprehensive two-dimensional experimental study conducted in a small-scale 1:50 wave flume. Results are presented for the overtopping performance at a 1 to 2 sloping wall, undertaken on both impermeable and permeable foreshore slopes. Within experimental limitations, the results demonstrate that the mean overtopping rate is reduced by up-to a factor of 4, when compared to the predictions reported for the impermeable slope. However, when comparing maximum individual wave-by-wave overtopping volumes, no significant differences were observed. These results are intended for practitioners and researchers predicting wave overtopping characteristics at sloping structures with permeable gravel foreshores.

Keywords

Overtopping discharge; Wave by Wave overtopping volume; Sediment rate; Shingle foreshore; Sloping wall.

*Corresponding Author

E-mail address: m.salauddin@warwick.ac.uk (M. Salauddin)

1. Introduction

The coastal zone is the interface between land and ocean where both natural and man-made hard or soft defences protect the hinterland areas against coastal flooding. Over the decades, conventional coastal engineering solutions result in hard structures such as seawalls, dykes and embankments. In addition to hard-engineering approaches, nature-based protection approaches, such as shingle beaches and barriers are also considered as an efficient coastal protection approach due to its natural capability to mitigate the wave induced energy (McCall et al., 2014).

Similar to other coastal infrastructures', shingle beaches and barriers can be affected by various wave induced hazards such as flooding due to extreme wave overtopping events (EurOtop, 2018). Hence, sea defences are usually designed to limit the wave induced overtopping at the structures during an extreme event. Many parametric experimental studies have been carried out to clarify the phenomenon of wave overtopping on coastal structures with fixed impermeable beaches, based on these predominantly small-scale laboratory measurements, several empirical formulae have been reported for the prediction of overtopping at these types of structures, e.g. EurOtop (2018).

There have been relatively few studies on the overtopping processes at shingle barriers and beaches, see Matias et al. (2012); Pearson (2010). For the prediction of cross-shore profile changes on a shingle coastline, many researchers proposed empirical prediction models, for instance predictions reported by Bradbury and Powell (1992); Lorang (2002); Van der Meer (1992); Van Hijum (1976); Van Hijum and Pilarczyk (1982). In additon, advances have also been made to compile large-scale datasets and to establish appropriate numerical methods for shingle beaches and barriers. To cite an example, to evaluate the morphological behaviour of shingle beaches and barriers, subjected to the action of waves, tides and storm, an extensive large-scale experimental investigation was undertaken, e.g. Williams et al. (2009), Williams et al. (2012a). Alongside the

experimental investigations, numerical studies on gravel beaches with the application of XBeach model have been performed by researchers, e.g. McCall et al. (2015); Williams et al. (2009); Williams et al. (2012b).

The vast majority of overtopping data applied in EurOtop (2018) has been derived from small-scale measurements with impermeable foreshore slopes. To date, there have been few parametric studies focussed on the investigation of the wave overtopping at sloping structures with a permeable foreshore slope. Recent laboratory work by Salauddin and Pearson (2019) demonstrated that average overtopping rates at a vertical breakwater on a shingle beach is reduced, when compared to the impermeable bed configuration. However, the overtopping performance of permeable gravel foreshores at sloping structures was not covered within the earlier work of Salauddin and Pearson (2019). There is a knowledge gap on the wave overtopping at sloping walls with permeable gravel slopes due to the lack of field and laboratory research on these types of sea defences.

The main purpose of this experimental research is to extend the existing empirical predictions of wave overtopping at smooth sloping structures for the case of permeable gravel foreshores. This paper extends the earlier research work of Salauddin and Pearson (2019), who investigated the wave overtopping at plain vertical walls with two permeable gravel foreshores subjected to impulsive and non-impulsive wave conditions. The extension presented in this article covers a comprehensive experimental study on the overtopping characteristics at 1 in 2 sloping structures, conducted on both impermeable and permeable foreshore slopes. Detailed results on the overtopping characteristics at sloping structures are presented and then compared with existing empirical predictions, which provide guidance for overtopping volumes at these types of sea

defences. These results are intended for practitioners and researchers predicting wave overtopping characteristics at sloping structures with permeable gravel foreshores.

2. Technical Background

2.1 Empirical Prediction of Overtopping

Wave overtopping or over-washing is one of the key hydraulic responses of a coastal structure (i.e. breakwater) due to its significant effects on the functional efficiency of a structure (Franco et al., 1994). For the design of a coastal defence, the design for tolerable wave overtopping is treated as one of the key concerns by researchers (EurOtop, 2018). At a coastal structure, an overtopping event mainly occurs when run-up heights of the largest waves are greater than the freeboard of the structure (TAW, 2002). The crest freeboard (R_c) is the vertical distance between the top of the structure and still water level line.

Mean overtopping discharge (q) in terms of per linear metre of width of the structure (l/m/s) is very often used to quantify wave overtopping phenomenon. Current prediction methods are based on a general exponential equation, which is used for describing wave overtopping discharge (q) on many coastal structures, including: vertical and sloping structures, armoured rubble mound breakwaters, coastal dikes, etc. (EurOtop, 2018; Franco et al., 1994; Owen, 1980). The exponential expression as formulated in Equation 1 is a special case of the Weibull-shaped function.

$$\frac{q}{\sqrt{gH_{m0}^3}} = a\exp(-b\frac{R_c}{H_{m0}}) \quad (1)$$

in which, q denotes average overtopping discharge, H_{m0} represents the significant wave height based on spectral analysis, a indicates the Weibull scale parameter, b exhibits the Weibull shape

parameter, R_c/H_{m0} is the dimensionless crest freeboard and $q/\sqrt{(gH_{m0}\text{^}3)}$ is defined the dimensionless wave overtopping discharge, e.g. EurOtop (2018).

The EurOtop overtopping manual was published in 2007 (EurOtop, 2007) based upon the most reliable existing empirical formulae from parametric tests. Further, Goda (2009) established a set of empirical formulations for the prediction of mean overtopping discharges at sloping structures by analysing the selected CLASH datasets and argued that new formulas (e.g. Equations 2-6) provide better prediction compared to those estimated by EurOtop (2007).

$$\frac{q}{\sqrt{gH_{m0}^3}} = \exp\left(-A - B\frac{R_c}{H_{m0}}\right) \quad (2)$$

where,

$$A = A_0 \tanh\left[(0.956 + 4.44\tan\theta).\left(\frac{h_t}{H_{m0}} + 1.242 - 2.032\tan^{0.25}\theta\right)\right] \quad (3)$$

$$B = B_0 \tanh\left[(0.822 - 2.22\tan\theta) \times \left(\frac{h_t}{H_{m0}} + 0.578 + 2.22\tan\theta\right)\right] \quad (4)$$

$$A_0 = 3.4 - 0.734\cot\propto + 0.239\cot^2\propto - 0.016\cot^3\propto \quad (5)$$

$$B_0 = 2.3 - 0.5\cot\propto + 0.15\cot^2\propto - 0.011\cot^3\propto \quad (6)$$

valid for $0 \leq \cot\propto \leq 7$

where, θ is the slope of the seabed, α is the slope of the structure and h_t is the toe water depth.

Later in 2014, Etemad-Shahidi and Jafari provided new formulas (Equations 7-8) for the prediction of mean overtopping rates at smooth impermeable sloping structures using a decision tree approach along with nonlinear regression model. They reported that the revised formulas outperform the existing empirical predictions for the estimation of overtopping at sloping structures.

$$\frac{q}{\sqrt{gH_{m0}^3}} = 0.032 \cdot \exp[-2.6\left(\frac{R_c}{H_{m0}}\right)^{1.6} \cdot (\xi_{m-1,0})^{-1.26}] \quad \text{for} \frac{R_c}{H_{m0}} \leq 1.62 \tag{7}$$

$$\frac{q}{\sqrt{gH_{m0}^3}} = 0.032 \cdot \exp[-5.63(\xi_{m-1,0})^{-1.26} - 3.283\left(\frac{R_c}{H_{m0}} - 1.62\right)^{0.83}] \quad \text{for} \frac{R_c}{H_{m0}} > 1.62 \tag{8}$$

Thereafter, Van der Meer and Bruce (2014) proposed a new set of formulae to predict overtopping at sloping structures both for breaking and non-breaking waves. They reported that the application of Goda's (2009) formulae should be limited to the slopes steeper than 1 in 2. They also reported that Goda's (2009) formulae will overestimate wave overtopping at gentle slopes with very low and zero crest freeboards.

The formulations of Van der Meer and Bruce (2014) were then incorporated into the updated overtopping manual, EurOtop (2018). For the estimation of mean overtopping discharges at smooth slopping walls under breaking and non-breaking wave conditions, EurOtop (2018) gives the following formulae, see Equations 9-10.

For breaking waves ($\xi_{m-1,0} < 2$)

$$\frac{q}{\sqrt{gH_{m0}^3}} = \frac{0.023}{\sqrt{\tan\alpha}} \cdot \xi_{m-1,0} \cdot \exp[-\left(2.7 \frac{R_c}{\xi_{m-1,0} \cdot H_{m0} \cdot \gamma_f}\right)^{1.3}] \tag{9}$$

For non-breaking waves ($\xi_{m-1,0} > \sim 2$) a maximum value of

$$\frac{q}{\sqrt{gH_{m0}^3}} = 0.09 \cdot \exp[-\left(1.5 \frac{R_c}{H_{m0}\, \gamma_f}\right)^{1.3}] \tag{10}$$

where,

γ_f = Influence factor for roughness elements on a slope [-]

It should be noted that for the smooth impermeable slope, the roughness factor equals to 1.0 in the above mentioned formulae (Equations 9-10). Breaker parameter or Iribarren number, $\xi_{m-1,0}$ is the combination of wave steepness and structure slope to distinguish breaking and non-breaking waves, see Equation 11. Equation 9 represents the estimation of overtopping for plunging or breaking waves ($\xi_{m-1,0} < \sim 2$), while Equation 10 denotes the maximum overtopping induced by non-breaking or surging waves ($\xi_{m-1,0} > \sim 2$), see EurOtop (2018) for a detailed explanation of breaking and non-breaking waves.

$$\xi_{m-1,0} = \frac{\tan\propto}{\sqrt{\frac{H_{m0}}{L_{m-1,0}}}} \quad (11)$$

where, α is the slope of the structure and $L_{m-1,0}$ is the deep water wave length based on spectral wave period $T_{m-1.0}$ ($=\frac{gT_{m-1,0}^2}{2\pi}$).

The maximum individual overtopping volume (V_{max}) in a known overtopping sequence can be calculated with the following formula (Equation 12).

Maximum individual overtopping volume (V_{max}),

$$V_{max} = a(\ln N_{ow})^{1/b} \quad (12)$$

where, V_{max} denotes the maximum wave by wave overtopping volume per meter width of the structure (m^3 per m), and N_{ow} represents the number of overtopping waves.

EurOtop (2018) recommended the following expression (Equation 8) for the estimation of Weibull scale factor, a,

$$a = \left(\frac{1}{\Gamma\left(1+\frac{1}{b}\right)}\right)\left(\frac{qT_m}{P_{ov}}\right) \quad (13)$$

where, T_m means average wave period, P_{ov} probability of overtopping waves and Γ denotes mathematical gamma function.

To determine the Weibull shape factor b at smooth sloping structures, Zanuttigh et al. (2013) suggested a new prediction formula (Equation 14) by presenting a relationship between shape factor and relative discharge ($q/(gH_{m0}T_{m-1,0})$.

$$b = 0.73 + 55\left(\frac{q}{gH_{m0}T_{m-1,0}}\right)^{0.8} \quad (14)$$

The number of overtopping waves (N_{ow}) can be approximated by knowing the probability of overtopping wave and total number of waves in a storm duration, see Equation 15 as recommended by EurOtop (2018).

$$P_{ov} = \frac{N_{ow}}{N_w} \quad (15)$$

For the estimation of the probability of overtopping waves (P_{ov}), Van der Meer and Janssen (1994) provided the following expression (Equation 16) by considering a Rayleigh distribution of the run-up heights and with the use of 2% run-up height ($R_{u2\%}$).

$$P_{ov} = \exp\left[-\left(\sqrt{-ln0.02}\,\frac{R_c}{R_{u2\%}}\right)^2\right] \quad (16)$$

For a relatively gentle slope with a breaker parameter less than $\xi_{m-1,0} \leq 4.0$, the following basic formula (Equation 17) can be applied to estimate the run-up heights at smooth sloping structures, e.g. TAW (2002).

$$\frac{R_{u2\%}}{H_{m0}} = 1.65\,\xi_{m-1,0} \quad (17)$$

The empirical formulae, Equation 16 and 17 as proposed by Van der Meer and Janseen (1994) and TAW (2002), respectively are also incorporated in the overtopping manual, e.g: EurOtop (2007); EurOtop (2018). It is important to note that these formulations are based on the measurement of run-up level which is usually calculated at a point on a straight slope but overtopping is measured on or behind the crest of the structure (EurOtop, 2018). Hence, EurOtop (2018) warned that these formulations always overestimate the number of overtopping waves.

Instead of using 2% run-up height ($R_{u2\%}$), Victor et. al. (2012) proposed another empirical expression (Equation 18) to estimate probability of overtopping at smooth impermeable slopes with the use of known relative freeboard and slope, subjected to non-breaking wave attack.

$$P_{ov} = \exp\left[-\left((1.4 - 0.30\cot\propto)\frac{R_c}{H_{m0}}\right)^2\right] \quad (18)$$

The existing prediction formulae currently available are principally founded on the fitting to experimental measurements, such as empirical formulae reported in the overtopping manual. Since most of the parametric studies were performed in the laboratory using an impermeable beach, uncertainties may exist in available prediction formulae when applied to permeable gravel slopes.

2.2 Scaling of shingle bed materials

To represent a gravel or shingle bed within the laboratory, crushed anthracite has been satisfactorily used as a model beach material by researchers over the years, e.g. Powell (1990), Coates and Dodd (1994). Powell (1990) described that the model bed materials should fulfil the following three requirements for the appropriate representation of the prototype beach, e.g. Salauddin and Pearson (2019).

— Beach permeability should be correctly reproduced in order to get the actual bed slope

— The threshold of motion has to be accurately replicated in order to find the minimum wave velocity to initiate the movement of the bed

— The relative magnitudes of the onshore and offshore movement should be precisely reproduced for evaluating whether the accretion or erosion occurs at the bed.

To fulfil these requirements, Powell (1990) proposed the methodology of Yalin (1963), Komar and Miller (1973) and Dean (1973) for the beach permeability, threshold of movement and, onshore and offshore movement criteria respectively. In summary, Powell (1990) reported the following formulations (Equations 19 – 22) to scale the model bed material.

— For accurate representation of permeability

$$\lambda_{\mathrm{D}} = \left(\frac{\lambda\, K_{\mathrm{p}}}{K}\right)\left(\frac{Re_{\mathrm{p}}}{\lambda^{\frac{1}{2}}\,\lambda_{\mathrm{D}}}\right) \tag{19}$$

— For accurate representation of onshore/offshore movement

$$\lambda_{\Delta} = \frac{\lambda\,\lambda_{\mathrm{CD}}}{\lambda_{\mathrm{D}}} \tag{20}$$

where,

$$\lambda_{\mathrm{CD}} = \left(\frac{C_{\mathrm{D_P}}}{C_D}\right)\left(\frac{Re_{\mathrm{p}}}{\lambda^{\frac{1}{2}}\,\lambda_{\mathrm{D}}}\right) \tag{21}$$

— For accurate threshold of motion

$$\lambda_{\Delta}\lambda_{\mathrm{D}}{}^{3/4} = \lambda^{3/4} \tag{22}$$

where, λ is the model scale, K_{p} and Re_{p} are the permeability and Reynolds number of the prototype situation, λ_{Δ} , Δ is $(\rho_{\mathrm{s}} - \rho_{\mathrm{f}})/\rho_{\mathrm{f}}$, ρ_{f} and ρ_{s} are the specific gravities of the fluid and sediment respectively, C_{D} is the drag coefficient and $C_{D\mathrm{p}}$ is the prototype drag coefficient. For known prototype values of K_{p} and Re_{p}, there are four equations to solve for four unknowns λ, λ_{D}, λ_{Δ} and λ_{CD}. As also mentioned by Powell (1990) that these four formulations can only be solved with the

assumption of prototype condition, which makes $\lambda = \lambda_D = \lambda_\Delta = \lambda_{CD}$ and subsequently three variables remain as unknown.

Another aspect is that the correct replication of all three criteria is practically unreachable since the model bed materials have only two characteristics (size and specific gravity of the sediments). In 1990, Powell found that the filtered anthracite materials with a quoted specific gravity of 1.39 justify most of the requirements by reproducing the correct magnitudes of onshore/offshore movement and threshold of motion. Later, this methodology was adapted by Coates and Dodd (1994) to scale down a narrow gravel bed d_{50} of 15 mm with a prototype density of 2.65 (T/m^3). These researchers concluded that at a 1:50 scaling filtered anthracite sediment d_{50} of 2.50 mm with a density of 1.40 (T/m^3) satisfy the most of the requirements to reproduce an assumed prototype gravel bed d_{50} of 15 mm. In this work, the mobile gravel beds were reproduced with the use of the crushed anthracite by adapting the methodology of Powell (1990).

3. Laboratory Set-Up

The laboratory set up for this experimental work has been performed by adapting the guidelines of EurOtop (2018) and Wolters et al. (2009) for typical two-dimensional wave flume investigations. The two-dimensional small-scale investigations were performed in a wave channel of 22 m long 0.60 m wide and 1.00 m deep (0.70 m operating depth), at the Warwick Water Laboratory. Experiments were carried out with a smooth impermeable 1: 2 sloping seawall on a uniform foreshore slope of 1 in 20, e.g. Fig. 1. A piston type wave paddle with an active wave absorption system is attached with the wave channel which is able to produce both irregular and uniform waves.

In this study, two different permeable 1 in 20 shingle foreshores were tested to investigate the overtopping characteristics at sloping structures with shingle foreshores. In addition to the shingle

beds, experiments were also undertaken with a uniform impermeable foreshore to study the wave overtopping at a sloping wall with a solid foreshore, which allowed comparison to previous studies, as reported in EurOtop, 2018.

To perform the experiments on permeable foreshores, two different gravel sediments were used and reproduced by crushed anthracite with a quoted specific gravity of 1.40, with the adaption of the well-known method of Powell (1990). Two different assumed prototype gravel slopes d_{50} of 13 mm and 24 mm with a prototype specific gravity of 2.65 (T/m^3) were reproduced with the use of two different sizes of model sediments. At a model length scale of 1:50, for assumed gravel beds d_{50} of 13 mm and 24 mm with a prototype specific gravity of 2.65 (T/m^3), the required sediment properties are listed in Table 1 with the application of expressions as suggested by Powell (1990) (Equations 19 –22). As observed in Table 1, the model sediment should have a specific gravity around 1.40 to satisfy the requirements of the correct magnitudes of onshore/offshore movement and threshold of motion. Hence, the filtered anthracite with a quoted specific gravity of 1.40 has been used in this study, which is also commercially available in various sizes. In Fig. 2, the grain size distribution curve of each gravel sediment is presented.

To measure the incident wave characteristics, a total of six wave gauges (resistance type) were used. Adopting the method suggested by Mansard and Funke (1980), the three-point technique was executed to separate the incident waves from reflected waves. The first set of three gauges were placed close to the wave generator, to measure the wave characteristics at comparatively deep water. In addition, three probes (number 4, 5 and 6 in Fig. 1) were positioned at the toe of the sloping structure to measure the inshore wave conditions. The gauge (number 6, Fig. 1) at the toe of the structure was set up adopting the method of Klopman and Van der Meer (1999) in order to reduce the influence of a reflective structure on the measured incident wave heights.

241 Although the paddle was equipped with an active absorption system to compensate the reflected
242 waves originating from the structure, due to the presence of reflections induced by structure, there
243 may be existence of uncertainties in the determination of incident inshore wave characteristics.
244 Thus, to reduce probable uncertainties in the measurement of inshore wave characteristics, the
245 measurements were also carried out by repeating the experiments without the existence of the
246 sloping walls in the flume (bare flume).

247 The overtopping discharges were determined using a load - cell technique by suspending a
248 measuring container behind the sloping wall from a calibrated load-cell, see Fig. 1. Wave by wave
249 overtopping events were identified by using two parallel strips of metal tape run along the crest of
250 the sloping wall which performed as a switch closed by the water. Individual overtopping volumes
251 were calculated by measuring the increment in the mass of overtopped water in the container after
252 each overtopping event for a test run.

253 A parameterized JONSWAP wave spectrum with a peak enhancement factor, $\gamma = 3.3$ ($\sigma_a = 0.07$
254 and $\sigma_b = 0.09$) was applied. Each experiment consisted of approximately 1000 random waves as
255 suggested by EurOtop (2018) and Wolters et al. (2009). This enabled the acquisition of the
256 measured overtopping characteristics which were statistically independent of the storm duration
257 (number of waves) for the experiment run.

258 Prior to running of each experiment with shingle bed configurations, the gravel foreshore slope
259 was reshaped to the initial beach profile of 1:20 in front of the sloping structure. Under the gravel
260 foreshore configurations, measurements of the scour hole depth at the toe of the sloping wall were
261 also carried out. Furthermore, for each test run, the bed level changes along the foreshore were
262 also investigated from the variation of initial and final elevation of the foreshore. From the

investigation on the development of scour depths with respect to storm durations, it was observed that an equilibrium profile can be achieved at around 1000 wave cycles, which are similar to studies by Sumer and Fredsøe (2000) at a 1 in 1.2 sloping wall on a sandy bed and Salauddin and Pearson (2019) at a plain vertical wall with permeable gravel foreshore.

Both low and high wave steepnesses were generated by performing experiments with two constant nominal deep-water wave steepnesses (s_{op}= 0.02 and 0.05). At a 1:50 scaling, the incident significant wave heights (H_{m0}) were tested from 50 mm to 160 mm and corresponding wave periods were in the range of 0.80 s to 2.26 s. Six different toe water depths were tested in this study. In total, around 180 test sequences were performed, see Table 2. Table 3 reports the nominal incident wave conditions followed in this research. It is noted that the nominal incident wave conditions as presented in Table 3 were applied to both impermeable and permeable slopes, indicating that one group of three tests was performed with the same incident wave condition with the three foreshores.

Furthermore, Table 4 shows the ranges of application for the sloping structure with impermeable and permeable slopes considered within this study. As it is seen in Table 4, the tested relative crest freeboards were in the range from 0.80 to 4.50 for both impermeable and permeable foreshore configurations. The minimum Iribarren number was equal to 2.0, indicating that tested wave conditions were non-breaking waves ($\xi_{m-1,0} > \sim 2$, EurOtop (2018)) on a relatively steep 1 in 2 smooth sloping structure.

4. Results and Analysis

4.1 Incident wave heights

In Fig. 3, two examples of measured incident wave heights at a relatively deep water (near wave paddle) are presented and compared with the deep-water Rayleigh distribution of wave heights. From the graph, it is noticeable that the measured wave heights overall follow the predicted Rayleigh distribution for both low and high wave steepnesses. There is, however, data points that correspond to relatively high waves that were found slightly lower than the prediction which may have occurred due to the occurrence of wave breaking near the wave paddle under depth-limited conditions.

4.2 Accuracy of measurement system

The accuracy of the overtopping measurement system was inspected prior to carrying out any experiments, adapting the technique followed by Pearson et al. (2001). A series of wave overtopping events were simulated by adding a known amount of water into the overtopping measuring tank. Then, the observed data from the overtopping detector and load-cell were processed by using an algorithm to find the number of overtopping waves and resulting individual overtopping volumes. Afterwards, the actual volume of each simulated overtopping event was compared with the measured value, e.g. Table 5. The test results clearly demonstrate that the measured overtopping volumes were almost identical to actual (given) values. The relative error of total measured volumes and actual volumes was found satisfactory around 0.7% and rmse (root mean square error) value was observed 9.38 ml indicating that any errors induced by the overtopping measurement technique were minimal. It is to note that the sensitivity of the load-cell was limited to the identification of 5-9 ml of overtopping volume, hence the smaller overtopping volumes showed an overall slightly greater error in the measurements compared to larger values.

4.3 Mean overtopping rate

In Fig. 4, the measured relative overtopping discharges $q/\sqrt{(gH_{m0}^3)}$ for the impermeable foreshore configuration (reference case) are compared with the predicted values, using the existing empirical predictions for sloping structures. To predict the mean overtopping rates, the empirical predictions of Goda (2009), Etemad-Shahidi and Jafari (2014) and EurOtop (2018) are presented in Fig. 4(a), 4(b) and 4(c) respectively. It can be seen from Fig. 4(a) that the predictions of the Goda (2009) formulae (Equations 2-6) overestimate the mean overtopping rates at sloping structures (1 in 2) for the tested conditions covered within this study. Similar characteristics of Goda's formulae for the prediction of mean overtopping rates at sloping structures with gentle slopes (milder than 1 in 2) were also reported by Van der Meer and Bruce (2014).

When comparing the results of the reference case with the empirical formulae of Etemad-Shahidi and Jafari (2014) and EurOtop (2018), it is seen that both the predictions of Etemad-Shahidi and Jafari (2014), Equations 7-8, and EurOtop (2018), Equations 9-10, overall succeed in providing the estimation of the mean overtopping rate, see Fig.4. However, it is also noticeable that the measured values overall show slightly better agreement with the predicted values of EurOtop (2018) compared to the those observed by Etemad-Shahidi and Jafari (2014).

For the quantitative comparison of the accuracy of the prediction formulae, the statistical error analysis such as root mean square error (rmse) and Bias analysis have been undertaken and reported in Table 6. The root mean square error (rmse) analysis and Bias analysis were performed with the use of measured and estimated values of overtopping using empirical formulations, as defined in Equations 23-24. As seen in Table 6, the prediction formulae of EurOtop (2018) outperforms the predictions of Etemad-Shahidi and Jafari (2014) and Goda (2009) by providing relatively lower rmse and Bias values for the tested impermeable bed configurations.

$$\text{rmse} = \sqrt{\frac{1}{N_{test}} \sum_{n=1}^{N_{test}} \left[\log\left(\frac{q_{measured}}{\sqrt{gH_{m0}^3}} \right)_n - \log\left(\frac{q_{predicted}}{\sqrt{gH_{m0}^3}} \right)_n \right]^2} \quad (23)$$

$$\text{Bias} = \frac{1}{N_{test}} \sum_{n=1}^{N_{test}} \left[\log\left(\frac{q_{predicted}}{\sqrt{gH_{m0}^3}} \right)_n - \log\left(\frac{q_{measured}}{\sqrt{gH_{m0}^3}} \right)_n \right] \quad (24)$$

in which, N_{test} is defined as the number of experimental results used to derive an equation. The smaller rmse-value means the better prediction formula which fits the specific dataset well. The rmse value demonstrates the standard deviation of the measured values about the mean predicted overtopping rates on a log-log scale.

The measured average overtopping rates for both impermeable (reference case) and gravel bed configurations are plotted in Fig. 5. The experimental results are compared with the prediction formulae (Equations 9-10) for sloping structures as reported by EurOtop (2018). The solid line in Fig. 5 represents the empirical expression of EurOtop (2018) considering an impermeable foreshore. The graph demonstrates that average overtopping discharges are reduced substantially for permeable gravel foreshore configurations compared to those observed for impermeable slope. From Fig. 5, it is also observed that the shingle foreshore of prototype grain diameter of 24 mm, provide a greater reduction in mean overtopping rate, when the two permeable bed configurations are compared.

An R^2 'best-fit' analysis was performed on the resulting average overtopping discharges to observe the reduction margin with the introduction of gravel foreshores compared to an impermeable slope, see Equations 25-26. It is noticeable that the overtopping is decreased by an approximate factor of 3.0 for gravel d_{50} of 13 mm and about a factor of 4.0 for d_{50} of 24 mm in comparison to the formulation (Equation 1) of EurOtop (2018). It is important to note that best-fit equations have

been derived by adapting the formulations of EurOtop (2018), which enables a direct comparison between new equations and existing empirical formulae.

For gravel d_{50} of 13 mm,

$$\frac{q}{\sqrt{gH_{m0}^3}} = 0.03 \cdot \exp\left[-\left(1.5\frac{R_c}{H_{m0}}\right)^{1.3}\right] \quad (25)$$

For gravel d_{50} of 24 mm,

$$\frac{q}{\sqrt{gH_{m0}^3}} = 0.0225 \cdot \exp\left[-\left(1.5\frac{R_c}{H_{m0}}\right)^{1.3}\right] \quad (26)$$

To investigate the reliability of the new equations, a root mean square error (rmse) analysis was performed with the use of measured and predicted values of overtopping using new equations (Equations 25-26), as following the approach applied by Owen (1980) and Victor et al. (2012), see Equation 23. In addition to rmse analysis, Bias analysis was also carried out to find the reliability of the derived equations, see Equation 24. In Table 7, the error measures of the proposed revised equations in the prediction of mean overtopping rate at sloping walls with permeable foreshores are shown.

For the conditions tested, the rmse value based on the measured and estimated values of overtopping was only 0.14 and 0.15 for gravel d_{50} of 13 mm (Equation 25) and d_{50} of 24 mm (Equation 26) respectively, see Table 7. Similar to rmse values, the observed Bias values for the new formulations were also smaller i.e; 0.03 for Equation 25 and 0.10 for Equation 26. These indicate that despite some scatter, in general, the predictions by using the revised expressions (Equations 25-26) exhibit a promising trend with the actual measurements.

Furthermore, in the prediction of overtopping at sloping structures, the effect of various factors such as influence of roughness factor of the armour slope, influence of berm, etc. in the reduction of overtopping is often incorporated by using a 'gamma factor' in the empirical expression, such as roughness factor of the sloping structure in Equation 10. To adopt a simple overall coefficient approach for the influence of permeable foreshore in the wave overtopping, measured mean overtopping rates are compared with various assumed foreshore roughness factors in Fig.6, using the empirical formulation of EurOtop (2018). The solid line represents the prediction of EurOtop (2018) considering a 'gamma factor' equals to 1.0 for the impermeable foreshore using Equation 10. Although, it is evident from the graph that test results of permeable foreshores do not perfectly fit with all data, using the "best-fit" empirical lines assuming foreshore roughness factors i.e.; 'gamma factor' of 0.70 (for d_{50} of 24 mm) and 0.80 (for d_{50} of 13 mm) using Equation 5. Nevertheless, an approximate trend is observed.

4.4 Mean overtopping sediment discharge

For the estimation of the average overtopping sediment rate, the mass of sediment overtopped in the collection tank was measured (dry weight), along with the mass of the water passing the parapet of the sloping wall. The dry weight of the sediments was then transformed to a volume with the use of the quoted specific gravity of 1.40 in order to make sure that the measurements were dimensionally comparable.

Fig. 7 illustrates the measured mean overtopping characteristics of the sediment and the overtopping characteristics of the water for the tested shingle foreshore configurations. The resulting data points demonstrate that the amount of sediment passes the parapet of the structure is approximately 1% of the amount of water. Also, it is noticeable from the graph that there is no

apparent effect of the size of the shingle foreshore slope on the overtopping of the sediment material at sloping seawall.

4.5 Distribution of wave by wave volumes

Wave by wave individual overtopping volumes in an overtopping sequence can be fitted with a Weibull distribution, e.g. Van der Meer and Jansen (1994); Besley (1999); Hughes et al. (2012). For robust predictions of maximum overtopping volumes, it is important to have a good distribution of wave by wave individual overtopping volumes. To examine the distribution of measured volumes, the observed individual overtopping volumes for each tested condition were investigated on a Weibull scale. Fig. 8 shows the resulting Weibull distribution of individual overtopping volumes for three distinct tested foreshore slopes for the same wave condition. In graph, V denotes wave by wave overtopping volume, $P(V)$ is the probability that an individual event volume equals or exceeds a volume V and V_{bar} represents average overtopping volume. The graph (Fig. 8d) provides a comparison of the distribution of overtopping volumes between impermeable and permeable foreshore slopes

From the gradient of linear regression line of the Weibull distribution, the Weibull b parameter can be calculated for an overtopping sequence. It has been demonstrated by many researchers that the higher individual overtopping volumes provide a good fit to the distribution with a reliable prediction of extreme wave by wave volumes, e.g. Pearson et al. (2002) and Zanuttigh et al. (2013). In general, the designers and practitioners are mainly interested on the largest individual overtopping volumes, hence, the shape factor b is usually determined by fitting only the extreme tail of the distribution (upper portion of the Weibull plot) using the relatively large overtopping volumes. In this study, the Weibull b has been determined for all the tested conditions by plotting a best-fitted trend line using the conventional fitting procedure i.e. upper part of the Weibull

412 distribution considering overtopping volumes greater than the average values ($V > V_{bar}$), as
413 indicated in Fig. 8.

414 Overall, the measured data points follow a linear trend, which indicates that the resulting wave by
415 wave volumes follow the Weibull distribution within this study, see Fig. 8a -8c. It is noticeable
416 from Fig. 8d, that the overtopping volumes distribution for different bed configurations are very
417 similar to each other which indicates that there is no obvious influence of gravel foreshore
418 configurations on the Weibull distribution of overtopping volumes.

419 **4.6 Proportion of waves overtopping**

420 The measured proportion of waves overtopping as a function of dimensionless freeboard is plotted
421 in Fig. 9. The graph compares the results of this study with the empirical prediction (Equation 18)
422 reported by Victor et al. (2012). The data points correspond to the benchmark tests represent the
423 experiments with the impermeable foreshore. These follow the Victor et al. (2012) prediction to
424 within a factor of 2. For the tested conditions, the measured proportion of waves overtopping was
425 reduced by an average of 50% for relative freeboards of 1.0 to 2.0 compared with the predictions,
426 whereas on an average 75% reduction was observed for relative freeboards of 2.0 to 3.5. When
427 comparing the two gravel slopes, it is noticeable that the larger gravel d_{50} of 24 mm, provides a
428 higher overall reduction in the proportion of waves overtopping.

429 In Fig. 10, the resulting proportion of overtopping waves are compared with the estimated values
430 (Equations 16-17) as reported by EurOtop (2018). For both impermeable and permeable
431 configurations, it is evident that the measured values are lower than the estimated values of
432 EurOtop (2018). As expected, this occurs due to the overestimation of the number of overtopping
433 waves by using the predictions of EurOtop (2018). An investigation of the time series, showed that

for the smaller waves such as for wave height of 50 mm for the model shingle d_{50} of 2.1 mm (H_{m0}/d_{50} ~ 25), the shingle beach was more 'efficient' in reducing the number of overtopping waves, and hence mean overtopping discharge rates.

4.7 Maximum overtopping volume

For the tested conditions, Fig. 11 compares the measured maximum overtopping wave volumes at sloping walls with the empirical prediction as suggested by Victor et al. (2012). The resulting data points correspond to both impermeable and gravel foreshore configurations approximately following the trend of that reported by Victor et al. (2012). It is evident that there is no discernible variation in the prediction of the maximum volumes for impermeable and permeable foreshores at sloping structures. Similar characteristics of the overtopping wave volumes with respect to different foreshore configurations were also reported by Salauddin and Pearson (2019) for vertical breakwaters with permeable shingle foreshores.

5. Discussion

A wide range of experiments were conducted in this study to inspect the overtopping characteristics at a smooth sloping structure on impermeable and permeable gravel foreshores and to provide the preliminary guidelines for the prediction of processes at full-scale. Generally, in the investigation of overtopping processes, Pearson et al. (2002) reported that the 'scale' and 'model' effects in the two-dimensional wave flume physical experiments showed no discernible differences in comparison to the large-scale laboratory measurements, for impermeable configurations (e.g. vertical walls). In addition, Victor and Troch (2012) concluded that for the smooth impermeable sloping structures, the influence of 'scale' effects is believed to be minimal in the wave overtopping measurements. In this study, the experimental set up has been complimented by adapting the well-established guidelines of EurOtop (2018), Powell (1990) and Wolters et al.

(2009) for typical two-dimensional experimental investigations. The tested significant wave heights were varied from 50 mm up to 160 mm, which were higher than the minimum wave heights of 30 mm as suggested by Wolters et al. (2009) to avoid 'scale' effects in the measurements. During the experiments, an active re-reflected wave absorber system was available in order to reduce the 'model' effects induced by reflection from the model boundaries. In addition, tests were complimented without the existence of any structure (bare flume) in the wave channel in order to validate the inshore wave conditions.

The measured incident wave conditions within this study overall follow the Rayleigh distribution at deep-water. The resulting overtopping from benchmark experiments (impermeable foreshore) showed a good agreement with the empirical prediction of EurOtop (2018). For both permeable and impermeable slopes, it was also observed that the distribution of wave by wave volumes follow the two-parameter Weibull distribution. Therefore, it is anticipated that the proposed revised prediction methods from this two-dimensional experimental research study, would be applicable at prototype conditions with minimal 'scale' and 'model' effects, even though the further validation of the dataset would be desirable.

6. Implications for Prediction Methods

To estimate the overtopping characteristics at a sloping wall on a gravel foreshore, to date, there are relatively limited prediction tools available in the literature. For a 'traditional' impermeable foreshore slope, the new manual EurOtop (2018) recommended Equations 9-10 for the estimation of average overtopping rates at sloping structures. It is important to note that to predict the mean overtopping discharges at sloping walls with permeable foreshores, the prediction guidance suggested in this study can be considered as a development of those described in the overtopping manual. Within the experimental limitations, the results of this study demonstrate that the average

480 overtopping discharge is reduced noticeably for permeable gravel beaches, when compared to an
481 impermeable slope (reference case). Therefore, a new set of prediction formulae (Equations 25-
482 26) is proposed in this study for the estimation of average overtopping rates at a 1 in 2 sloping wall
483 with a permeable gravel 1 in 20 foreshore configuration. A conservative method is suggested, i.e.
484 an impermeable slope, see empirical expressions (Equations 9-10) as described by EurOtop
485 (2018), when there is no other information available.

486 For the estimation of the average sediment discharges at a sloping structure on a permeable shingle
487 beach, to date, there is no guidance available. Based on an analysis of the measured average
488 sediment discharge, it is recommended to expect up to 1% of the sediment material within the
489 overtopping waves.

490 As observed in Fig. 10, the measured values of probability of overtopping waves at a sloping
491 structure on a gravel foreshore were lower compared to the impermeable foreshore. However, the
492 measured maximum individual wave overtopping volumes for shingle beaches do not vary
493 significantly (within a factor of 2) from those obtained for impermeable slopes, as shown in Fig.
494 11. A correlation between overtopping wave volumes and number of overtopping waves for both
495 impermeable and shingle beds is presented in Fig 12., also shown is a comparison of the
496 distribution of overtopping volumes for various foreshore configurations for an incident wave
497 height (H_{m0}) of 100 mm with a wave steepness ($s_{m-1,0}$) of 0.06. It is noticeable that for the
498 impermeable foreshore configuration, a higher number of overtopping waves compared to the
499 shingle foreshores for the same wave condition is observed. For example, the data points
500 corresponding to the solid foreshore slope represent around 49% of overtopping waves, while the
501 shingle bed d_{50} of 13 mm and d_{50} of 24 mm provide about 33% and 32% respectively.

It is however noticeable that the maximum wave by wave overtopping volumes on gravel beds overall do not differ significantly from those reported on impermeable beach configuration. For instance, the graph (Fig. 12) shows that the maximum individual overtopping volume of 3.0 litre per m width for the impermeable foreshore and 2.9 litre per m width for shingle bed d_{50} of 13 mm. This indicates that permeable shingle beaches lead to less wave overtopping events, and hence lower mean overtopping discharges, but the maximum individual overtopping volumes are similar for both cases. Considering the random characteristics of wave by wave overtopping volumes, the updated EurOtop manual (EurOtop 2018) also emphasized the significance of the influence of individual overtopping volumes on the tolerable overtopping discharges. We therefore recommend a conservative prediction of maximum individual overtopping volumes at sloping walls with permeable shingle beaches i.e. the predictions as stated by EurOtop (2018) considering a solid foreshore slope is suggested.

7. Conclusions

The average overtopping discharge, average sediment discharge, proportion of overtopping waves and, wave by wave overtopping volumes on a sloping structure, for both impermeable and permeable gravel foreshore configurations have been studied based on the experimental results and through a comparison with existing empirical formulations from literature. Our conclusions are summarised as follows:

— The measured baseline overtopping characteristics corresponding to the impermeable beach configuration (control condition) correlated well with the existing predictions for the tested conditions.

— The results on mean overtopping discharge showed that the overtopping is reduced for permeable foreshore slopes in comparison to impermeable slopes. A reduction factor of 3.0 and 4.0 was reported for the gravel bed d_{50} (prototype) of 13 mm and d_{50} of 24 mm respectively.

— The measured volume of overtopped sediment was found approximately 1% of the total overtopping volume for the conditions covered within this study.

— For the tested conditions, the measured proportion of waves reduced by an average of 50% for relative freeboards of 1.0 to 2.0 compared with the empirical predictions, whereas on an average 75% reduction was observed for relative freeboards of 2.0 to 3.5.

— The measured values of wave by wave and maximum overtopping volumes for shingle beaches were somewhat similar (within a factor of 2) to those measured for impermeable slopes. This indicates that there is no obvious influence of gravel foreshore configurations on the Weibull distribution of overtopping volumes as well as on the maximum individual overtopping volumes for the conditions tested within this study.

For the prediction of overtopping characteristics at sloping structures on permeable gravel foreshores, a revised predictions tool is suggested.

Acknowledgements

This work was funded by the University of Warwick: Chancellor's International Scholarship. The laboratory work was financially supported through the Leverhulme Trust Senior Research Fellowships scheme (2016/2017) of the Royal Academy of Engineering (Ref: LTSRF1516\12\92). The authors also would like to thank the Natural Environmental Research Council (Grant Ref.: NE/RE003645/1) for the financial support for providing the advanced wave analysis tools. The

545 constructive comments and suggestions by the anonymous reviewers are greatly appreciated in
546 improving this manuscript.

547

548

549 ## Notation

Symbol	Meaning	Unit
a	Scale parameter in Weibull distribution	[-]
b	Shape parameter in Weibull distribution	[-]
d_{50}	Mean sediment size	[mm]
g	Gravitational acceleration	[m/s^2]
h	Water depth at toe of the structure	[m]
H_{m0}	Significant wave height determined from spectra analysis	[m]
$L_{m-1,0}$	Spectral wave length based on linear theory ($gT_{m-1,0}^2/2\pi$)	[m]
N_{ow}	Number of overtopping waves	[-]
N_w	Number of incident waves	[-]
P_{ov}	Probability of overtopping per wave (N_{ow}/N_w)	[-]
P(V)	Probability of exceedance of overtopping volume	[-]
q	Mean overtopping discharge per m width	[m^3/s per m]
R_c	Crest freeboard	[m]
R_u	Run-up level exceeded by 2% of incident waves	[m]
$s_{m-1,0}$	Wave steepness based on mean spectral period ($2\pi H_{m0}/gT_{m-1,0}^2$)	[-]
s_{op}	Wave steepness for spectral peak period ($2\pi H_{m0}/gT_p^2$)	[-]
T_m	Average wave period calculated from time series analysis	[s]
$T_{m-1,0}$	Average spectral wave period defined from spectral analysis by m_{-1}/m_0	[s]
T_p	Spectral peak wave period	[s]
V	Volume of overtopping wave per m width	[m^3 per m]
V_{bar}	Mean overtopping volume per m width	[m^3 per m]
V_{max}	Maximum individual overtopping volume per m width	[m^3 per m]
α	Slope of the structure	[radians]
γ	Peak enhancement factor of JONSWAP energy spectrum	[-]
λ	Model scale	[-]
$\xi_{m-1,0}$	Breaker parameter	[-]
Γ	Mathematical gamma function	[-]

550

References

Besley, P. 1999. Overtopping of seawalls – design and assessment manual. R&D Technical Report W 178, Environment Agency, UK. ISBN 1 85705 069 X.

Bradbury, A., Powell, K., 1992. The short term profile response of shingle spits to storm wave action. In: Proceedings of 23rd International Conference on Coastal Engineering, ASCE, pp. 2694-2707.

Bradbury, A., 2000. Predicting breaching of shingle barrier beaches-recent advances to aid beach management. In: Proceedings of the 35th Annual MAFF Conference on River and Coastal Engineering, pp. 05.3.1-05.3.13.

Coates, T. T., Dodd, N, 1994. The response of gravel beaches in the presence of control structures. In: Proceedings of Coastal Engineering, Kobe, Japan. ASCE, pp. 1880-1894.

Dean, R. G., 1973. Heuristic Models of Sand Transport in the Surf Zone. In: Proceedings of the Conference on Engineering Dynamics in the Surf Zone, Institution of Civil Engineers, Australia, Sydney, pp. 208-214.

De San Román-Blanco, B. L., Coates, T. T., Holmes, P., Chadwick, A. J., Bradbury, A., Baldock, T. E., Pedrozo-Acuna, A., Lawrence, J., Grüne, J., 2006. Large scale experiments on gravel and mixed beaches: Experimental procedure, data documentation and initial results. Coastal Engineering 53(4), 349-362.

Etemad-Shahidi, A., Jafari, E. 2014. New formulae for prediction of wave overtopping at inclined structures with smooth impermeable surface. Ocean Engineering, 84, 124-132.

EurOtop, 2007. Wave Overtopping of Sea Defences and Related Structures: Assessment Manual. Expertise Netwerk- UK: N. W. H. Allsop, T. Pullen, T. Bruce. NL: J. W. Van der Meer. DE: H. Schüttrumpf, A. Kortenhaus.

574 EurOtop, 2018. Manual on wave overtopping of sea defences and related structures. Second
575 Edition. (Available to download from www.overtopping-manual.com).
576 Franco, L., De Gerloni, M., Van Der Meer, J., 1994. Wave overtopping on vertical and composite
577 breakwaters. In: Proceedings of the 24th ICCE, ASCE, Kobe, Japan, pp. 1030-1045.
578 Goda, Y., 2009. Derivation of unified wave overtopping formulas for seawalls with smooth,
579 impermeable surfaces based on selected CLASH datasets. Coastal Engineering 56(4), 385-
580 399.
581 Holthuijsen, L. H., 2007. Waves in oceanic and coastal waters. Cambridge University Press,
582 Cambridge.
583 Hughes, S. A., Thornton, C. I., Van der Meer, J.W., Scholl, B. N., 2012. Improvements in
584 describing wave overtopping processes. In: Proceedings of ICCE 2012, ASCE, Santander,
585 Spain.
586 Klopman, G. and Van der Meer, J.W., 1999.Random wave measurements in front of reflective
587 structures. Journal of Waterway Port Coast and Ocean Engineering 125 (1), pp. 39-45.
588 Komer, P. D. and Miller, M. C., 1973. The threshold of sediment movement under oscillatory
589 water waves. Journal of Sedimentary Petrology 43(4), pp. 1101-1110.
590 Lorang, M. S., 2002. Predicting the crest height of a gravel beach. Geomorphology, 48(1), 87-101.
591 Mansard, E.P.D., Funke, E.R., 1980. The measurement of incident and reflected spectra using a
592 least squares method. Coastal Engineering 154–172.
593 Matias, A., Williams, J. J., Masselink, G., Ferreira, Ó., 2012. Overwash threshold for gravel
594 barriers. Coastal Engineering 63, 48-61.

McCall, R. T., Masselink, G., Poate, T. G., Roelvink, J. A., Almeida, L. P., Davidson, M. & Russell, P. E., 2014. Modelling storm hydrodynamics on gravel beaches with XBeach-G. Coastal Engineering, 91, 231-250.

McCall, R., Masselink, G., Poate, T., Roelvink, J., Almeida, L., 2015. Modelling the morphodynamics of gravel beaches during storms with XBeach-G. Coastal Engineering 103, 52-66.

Owen, M. W., (1980). Design of sea walls allowing for wave overtopping. Report EX 924, Hydraulics Research Station, Wallingford, UK.

Pearson, J. M., Bruce, T., Allsop, N. W. H.,2001. Prediction of wave overtopping at steep seawalls—variabilities and uncertainties. In: Proceedings of the Conference on Waves '01, San Francisco, ASCE, pp. 1797-1808.

Pearson, J. M., Bruce, T., Allsop, N. W. H., Gironella, X., 2002. Violent wave overtopping-measurements at large and small scale. In: Proceedings of the 28th International Coastal Engineering Conference, ASCE, Cardiff, UK, pp. 2227-2238.

Pearson, J. M., 2010. Overtopping and Toe Scour at Vertical Seawalls. In: Proceedings of the 9th international conference on Coasts, marine structures and breakwaters: Adapting to change, Institution of Civil Engineers, Thomas Telford Ltd, Edinburgh, pp. 598-608.

Powell, K. A., 1990. Predicting short term profile response for shingle beaches. Report SR 219, HR Wallingford,Wallingford, UK.

Salauddin, M., Pearson, J. M., 2019. Wave overtopping and toe scouring at a plain vertical seawall with shingle foreshore: A Physical model study. Ocean Engineering 171, 286-299.

Sumer B.M., Fredsøe J., 2000. Experimental study of 2D scour and its protection at a rubble-mound breakwater. Coastal Engineering 40, 59–87.

618 TAW, 2002. Technical report wave run-up and wave overtopping at dikes. In: Van der Meer, J.
619 W. (ed) TAW report (incorporated in the EurOtop manual).
620 Van der Meer, J. W., 1992. Stability of the seaward slope of berm breakwaters. Coastal
621 Engineering 16(2), 205-234.
622 Van der Meer, J.W., Janssen, J.P.F.M., 1994. Wave run-up and wave overtopping at dikes. In:
623 Wave forces on inclined and vertical wall structures, ed. N. Kobayashi and Z. Demirbilek,
624 ASCE, pp. 1-27.
625 Van der Meer, J. W., Bruce, T., 2014. New physical insights and design formulas on wave
626 overtopping at sloping and vertical structures. Journal of Waterway, Port, Coastal, and
627 Ocean Engineering 140(6), 04014025.
628 Van Hijum, E., 1976. Equilibrium profiles and longshore transport of coarse material under
629 oblique wave attack. In: Proceedings of 15th Conference on Coastal Engineering,
630 Honolulu, Hawai.
631 Van Hijum, E., Pilarczyk, K., 1982. Equilibrium profile and longshore transport of coarse material
632 under regular and irregular wave attack. Publication No. 174, Delft Hydraulics laboratory,
633 Delft, Netherlands.
634 Victor, L., Troch, P., 2012. Wave overtopping at smooth impermeable steep slopes with low crest
635 freeboards. Journal of Waterway, Port, Coastal, and Ocean Engineering, 372–385.
636 Victor, L., Van der Meer, J. W., Troch, P., 2012. Probability distribution of individual wave
637 overtopping volumes for smooth impermeable steep slopes with low crest freeboards.
638 Coastal Engineering 64, 87-101.

639 Williams, J. J., Masselink, G., Buscombe, D., Turner, I., Matias, A., Ferreira, O., Bradbury, A.,
640 Metje, N., Coates, L., Chapman, D., 2009. BARDEX (Barrier Dynamics Experiment):
641 taking the beach into the laboratory. Journal of Coastal Research, 158-162.
642 Williams, J. J., Buscombe, D., Masselink, G., Turner, I., Swinkels, C., 2012a. Barrier Dynamics
643 Experiment (BARDEX): aims, design and procedures. Coastal Engineering 63, 3-12.
644 Williams, J. J., De Alegría-Arzaburu, A. R., McCall, R. T., Van Dongeren, A., 2012b. Modelling
645 gravel barrier profile response to combined waves and tides using XBeach: Laboratory and
646 field results. Coastal Engineering 63, 62-80.
647 Wolters, G., Van Gent, M., Allsop, N. W. H., Hamm, L., Mühlestein, D., 2009. HYDRALAB III:
648 Guidelines for physical model testing of rubble mound breakwaters. In: Proceedings of the
649 9th International Conference on Coasts, Marine Structures and Breakwaters: Adapting to
650 Change, Edinburgh, United Kingdom, pp. 659-670.
651 Yalin, S., 1963. A model shingle beach with permeability and drag forces reproduced. In:
652 Proceedings of the 10th IAHR Congress 1963. London pp.169.
653 Zanuttigh, B., Van Der Meer, J. W., Bruce, T., Hughes, S., 2013. Statistical characterisation of
654 extreme overtopping wave volumes.In: Proceedings of ICE, Coasts, Marine Structures and
655 Breakwaters, Edinburgh, UK.
656
657

List of Tables

Table 1

Properties of model bed materials

Prototype d_{50} [mm]	Model Scale	Model d_{50} [mm]	Sp. Gravity of sediment ρ_s [T/m^3] for threshold of motion	Sp. Gravity of sediment ρ_s [T/m^3] for onshore or offshore movement
13	1:50	2.1	1.42	1.39
24	1:50	4.2	1.45	1.37

662 **Table 2**

663 Overview of test matrix

Type of foreshore slope	Water depth, h_t [mm]	Crest freeboard, R_c [mm]	Spectral wave height, H_{m0} [mm]	Nominal wave steepness, s_{op} [-]	Wave Period, T_p [s]
Impermeable	60	190	50-160	0.02	1.27-2.26
				0.05	0.80-1.43
Impermeable	75	245	50-160	0.02	1.27-2.26
				0.05	0.80-1.43
Impermeable	100	150	50-160	0.02	1.27-2.26
				0.05	0.80-1.43
Impermeable	150	100	50-160	0.02	1.27-2.26
				0.05	0.80-1.43
Impermeable	180	140	50-160	0.02	1.27-2.26
				0.05	0.80-1.43
Impermeable	200	50	50-160	0.02	1.27-2.26
				0.05	0.80-1.43
Permeable shingle (d_{50} = 13 mm / d_{50} = 24 mm)	60	190	50-160	0.02	1.27-2.26
				0.05	0.80-1.43
Permeable shingle (d_{50} = 13 mm / d_{50} = 24 mm	75	245	50-160	0.02	1.27-2.26
				0.05	0.80-1.43
Permeable shingle (d_{50} = 13 mm / d_{50} = 24 mm	100	150	50-160	0.02	1.27-2.26
				0.05	0.80-1.43
Permeable shingle (d_{50} = 13 mm / d_{50} = 24 mm	150	100	50-160	0.02	1.27-2.26
				0.05	0.80-1.43
Permeable shingle (d_{50} = 13 mm / d_{50} = 24 mm	180	140	50-160	0.02	1.27-2.26
				0.05	0.80-1.43
Permeable shingle (d_{50} = 13 mm / d_{50} = 24 mm	200	50	50-160	0.02	1.27-2.26
				0.05	0.80-1.43

664

665

666

667

Table 3

Nominal wave conditions

	T_p [sec]									
s_{0p} [-] /H_{m0} [mm]	50	55	60	70	80	90	100	120	140	160
0.02	1.27	1.33	1.39	1.50	1.60	1.70	1.79	1.96	2.12	2.26
0.05	0.80	0.84	0.88	0.95	1.01	1.07	1.13	1.24	1.34	1.43

Table 4

Ranges of application for the sloping structure with permeable foreshore considered within this study

Minimum		Parameter		Maximum
0.80	≤	Relative Freeboard, R_c/H_{m0}	≤	4.5
0.015	≤	Wave Steepness, s_{op}	≤	0.05
2.0	<	Irribaren Number, Ir		
2.0	=	Slope of the structure, Cotα		

677 **Table 5**

678 A comparison between the actual volume and measured volume using the overtopping
679 measurement system

No .of event	Actual Volume (ml)	Measured Volume (ml)	Actual error (ml)	Relative error (%)	RMSE (ml)
1	25	21	-4	-16.0	9.38
2	50	45	-5	-10.0	
3	75	78	3	4.0	
4	100	93	-7	-7.0	
5	175	181	6	3.4	
6	200	189	-11	-5.5	
7	300	289	-11	-3.7	
8	500	511	11	2.2	
9	750	742	-8	-1.1	
10	1000	988	-12	-1.2	
11	1250	1237	-13	-1.0	
12	1500	1489	-11	-0.7	
13	1250	1258	8	0.6	
14	1000	1008	8	0.8	
15	500	486	-14	-2.8	
Total	**8675**	**8615**	**-60**	**0.7**	**9.38**

680

681

Table 6

The error measures of existing empirical equations for the prediction of overtopping rates at a sloping wall with an impermeable foreshore

Error Indicator	Goda (2009) – Eqns. (2-6)	Etemad-Shahidi and Jafari (2014) – Eqns. (7-8)	EurOtop (2018) – Eqn. (10)
rmse	0.60	0.26	0.12
Bias	0.38	0.09	0.007

Table 7

The error measures of proposed equations for the prediction of overtopping rates at sloping walls with permeable foreshores

Error Indicator	Eqn. 25 (Gravel d_{50} of 13 mm)	Eqn. 26 (Gravel d_{50} of 24 mm)
rmse	0.14	0.15
Bias	0.03	0.10

List of Figures

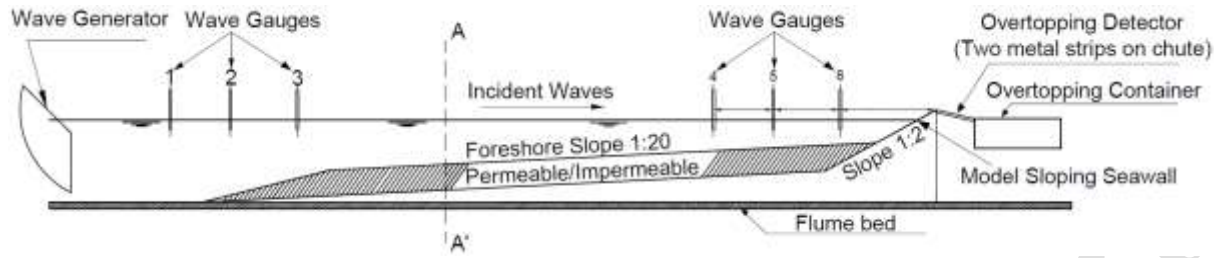

a.

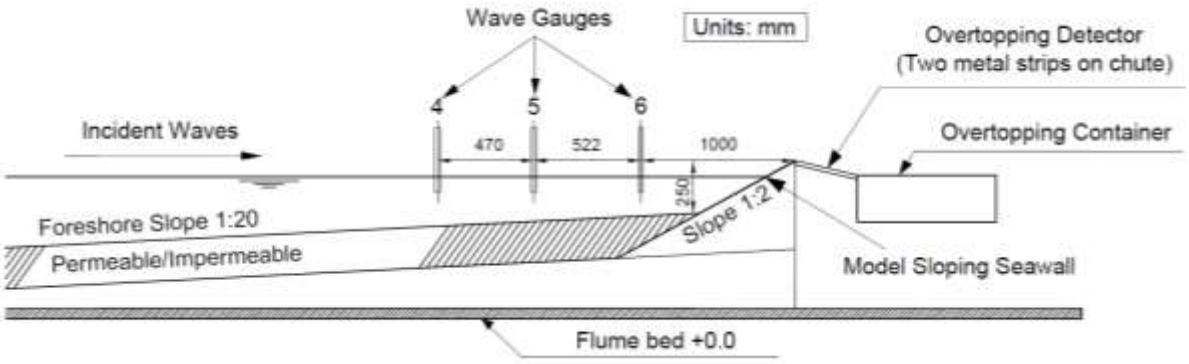

b.

c.

Fig. 1. Experimental set –up a. Cross-section along the length of wave channel, b. The overtopping measurement techniques and location of wave gauges (A-A'), c. Photograph of an experiment with shingle foreshore d_{50} of 13 mm

701

a.

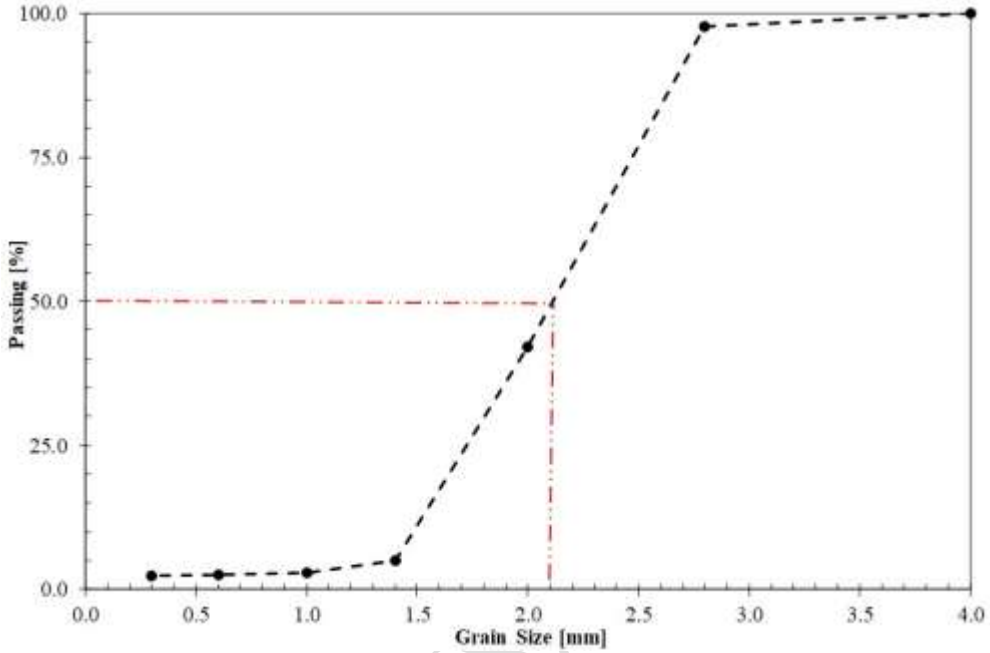

b.

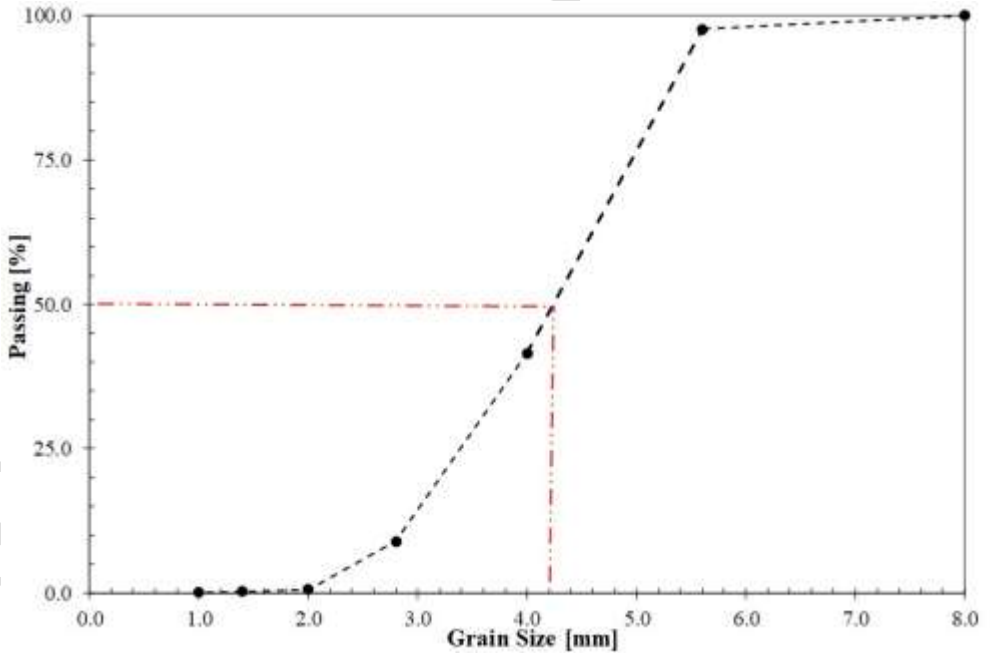

702 **Fig. 2.** The grain size distribution curves of shingle anthracites - a) d_{50} of 2.10 mm b) d_{50} of 4.20

703 mm; as used in Salauddin and Pearson (2019)

704

a.

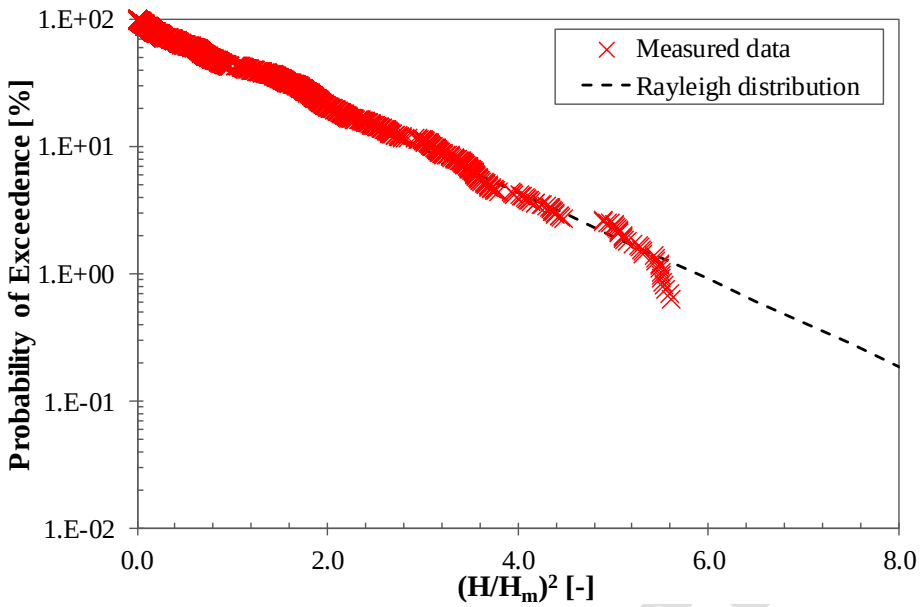

b.

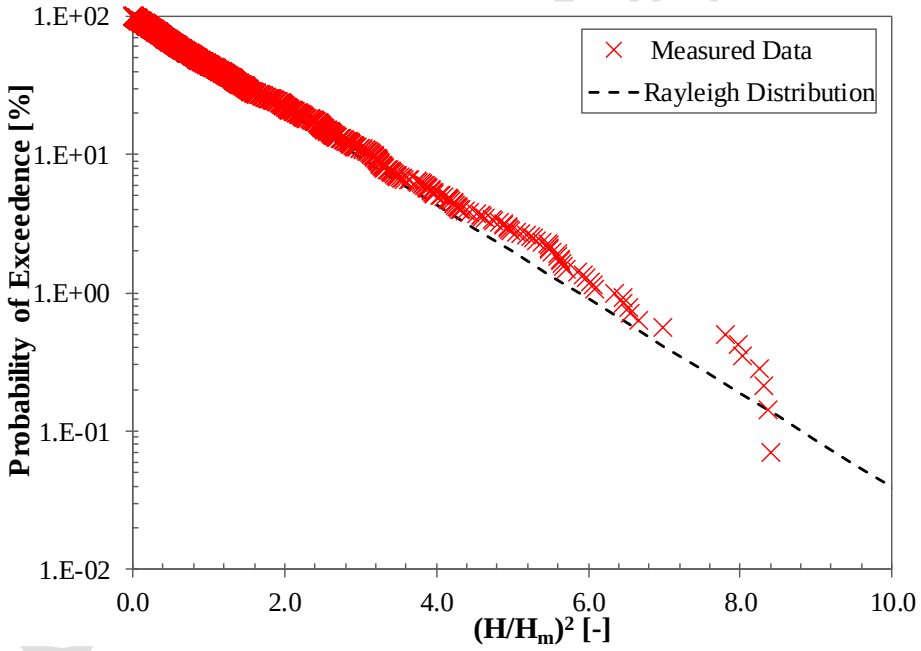

705 **Fig. 3.** A comparison between measured and predicted distribution of incident wave heights - a)

706 $s_{m-1,0} = 0.02$, $H_{m0} = 70$ mm b) $s_{m-1,0} = 0.06$, $H_{m0} = 100$ mm

707

a.

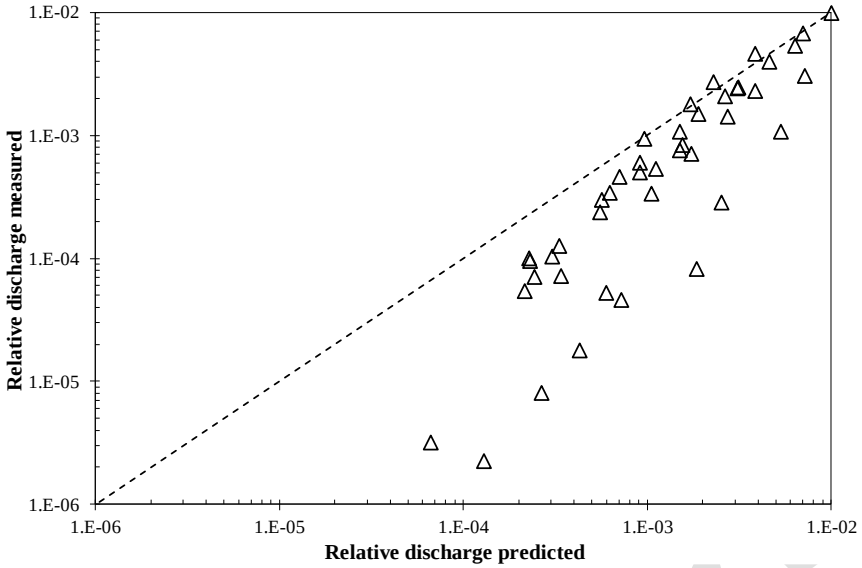

b.

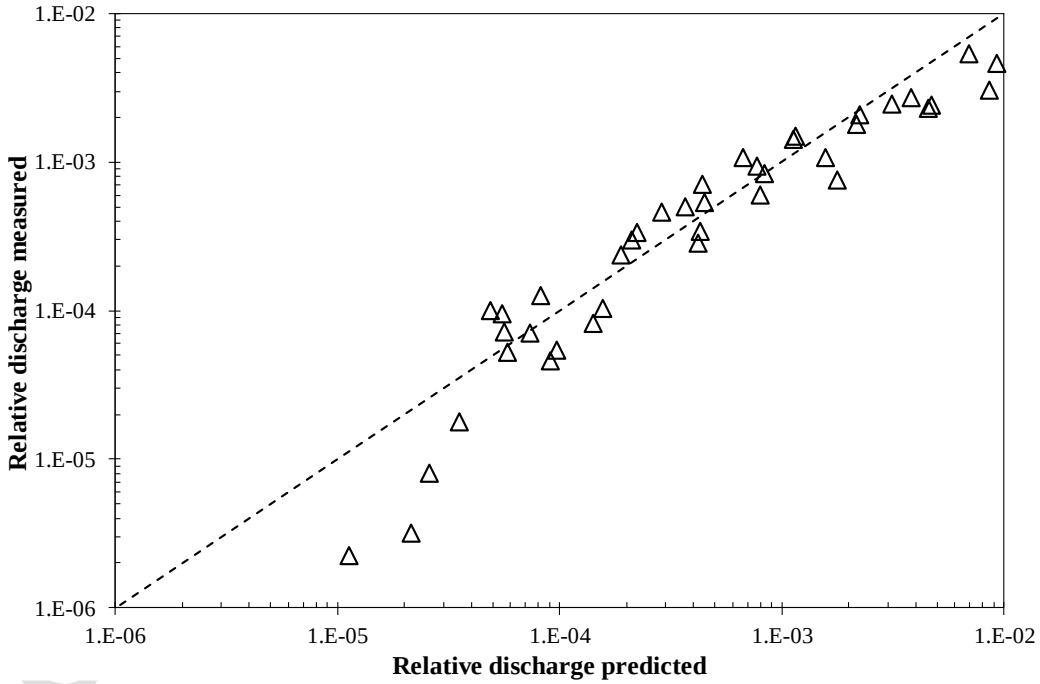

c.

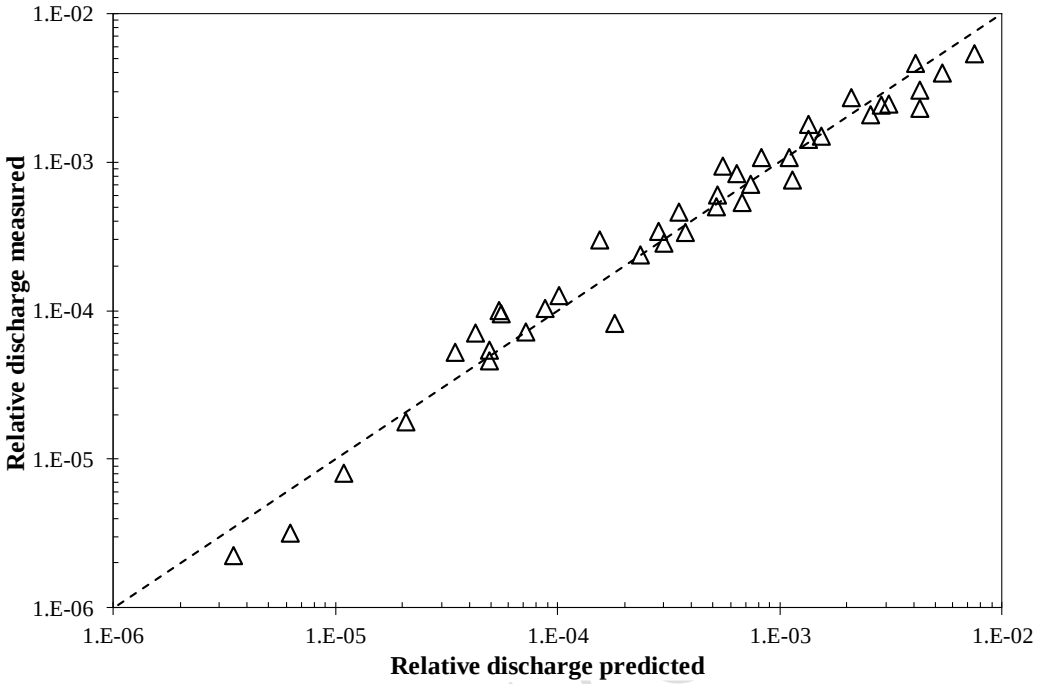

Fig. 4. Measured relative overtopping discharges at a sloping wall on an impermeable foreshore, compared to the prediction of a) Goda (2009), b) Etemad-Shahidi and Jafari (2014) and c) EurOtop (2018)

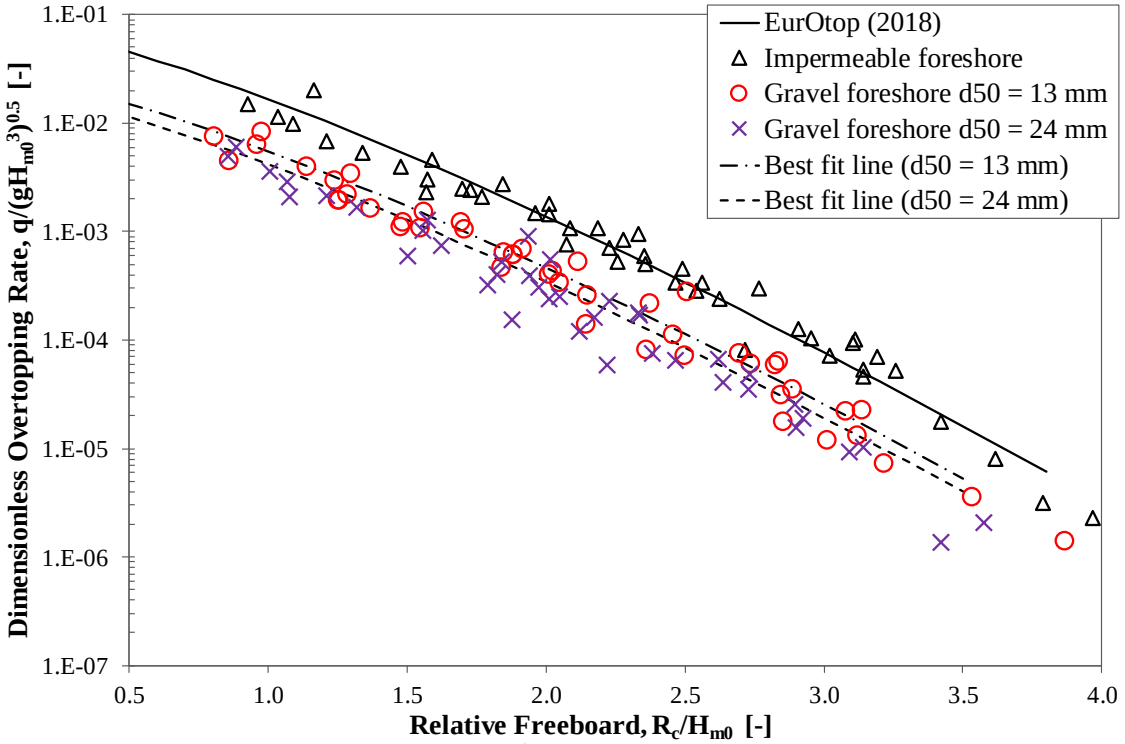

712 **Fig. 5**. Dimensionless average overtopping rate against relative freeboard at sloping walls

713

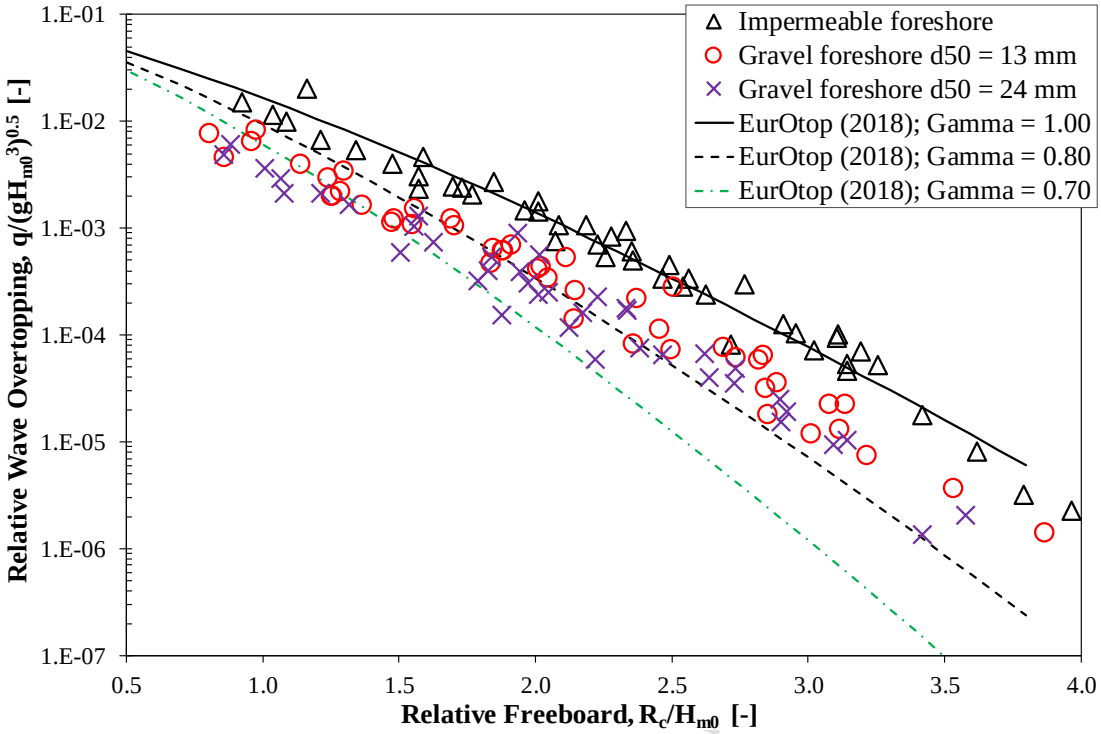

714 **Fig. 6**. Estimation of roughness factor for the influence of permeable foreshore

715

716

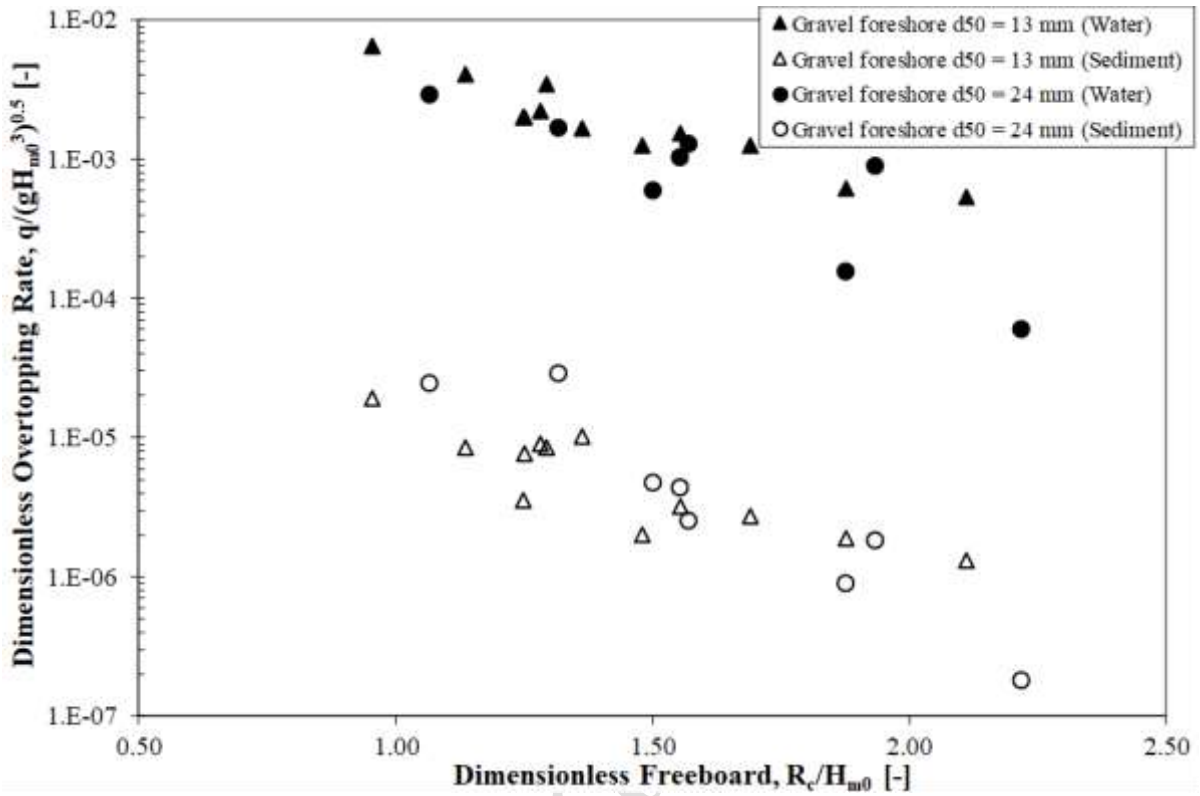

717

718 **Fig. 7.** A comparison between average overtopping rate of water and sediment at sloping walls

719

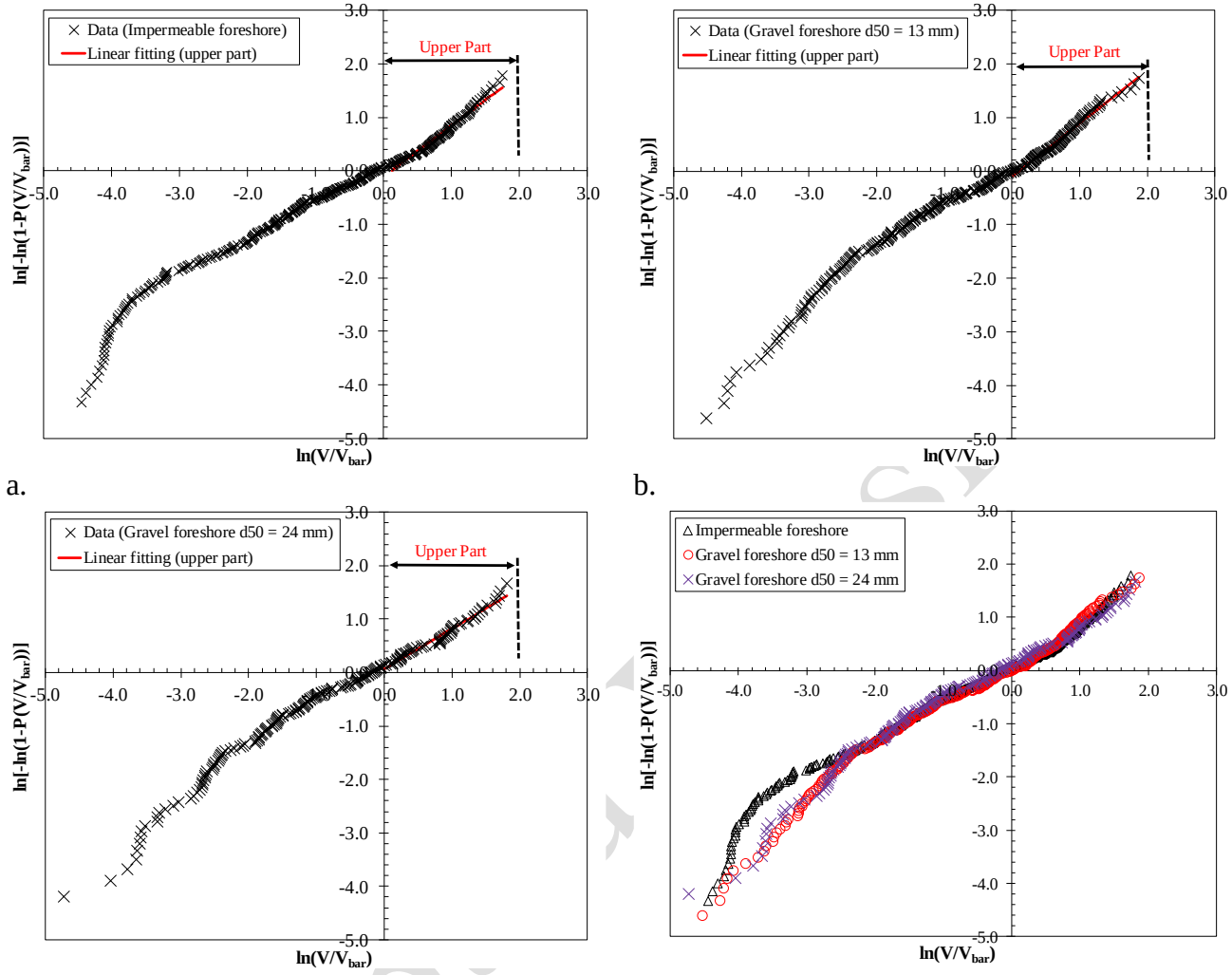

720 **Fig. 8.** Weibull distribution of individual overtopping volumes for an incident significant wave
721 height (H_{m0}) of 70 mm with a wave steepness ($s_{m-1,0}$) of 0.02 - a) Impermeable foreshore b) Gravel
722 foreshore d_{50} = 13 mm and c) Gravel foreshore d_{50} = 24 mm and d) Variation of wave by wave
723 volumes at sloping structures with different foreshore configurations

724

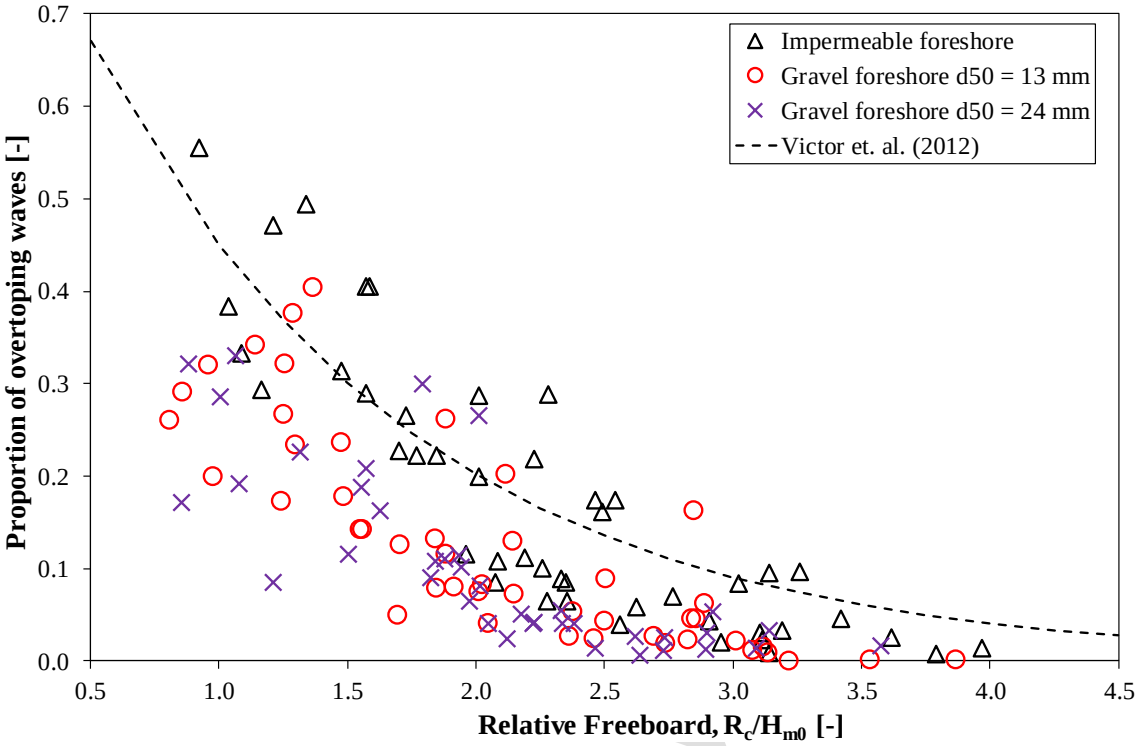

725 **Fig. 9**. Proportion of overtopping waves at sloping structures for both impermeable and

726 permeable foreshore configurations

727

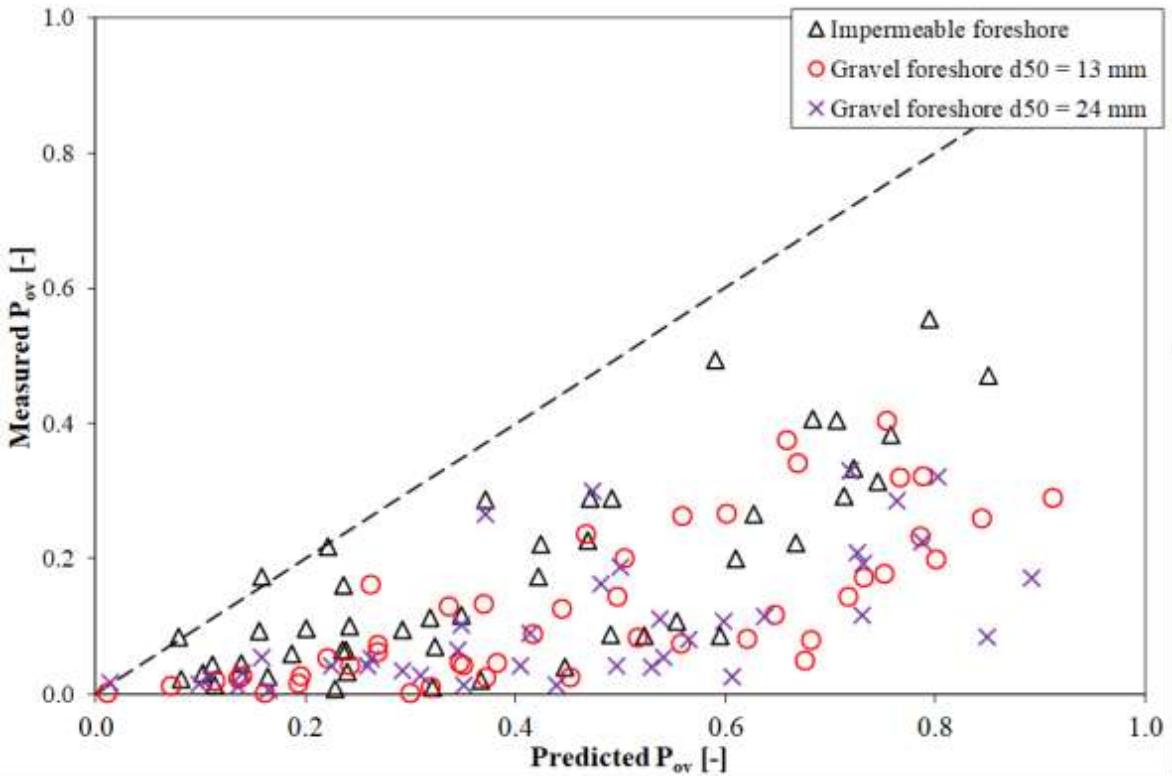

728 **Fig. 10.** A comparison of measured and predicted proportion of overtopping waves

729

730

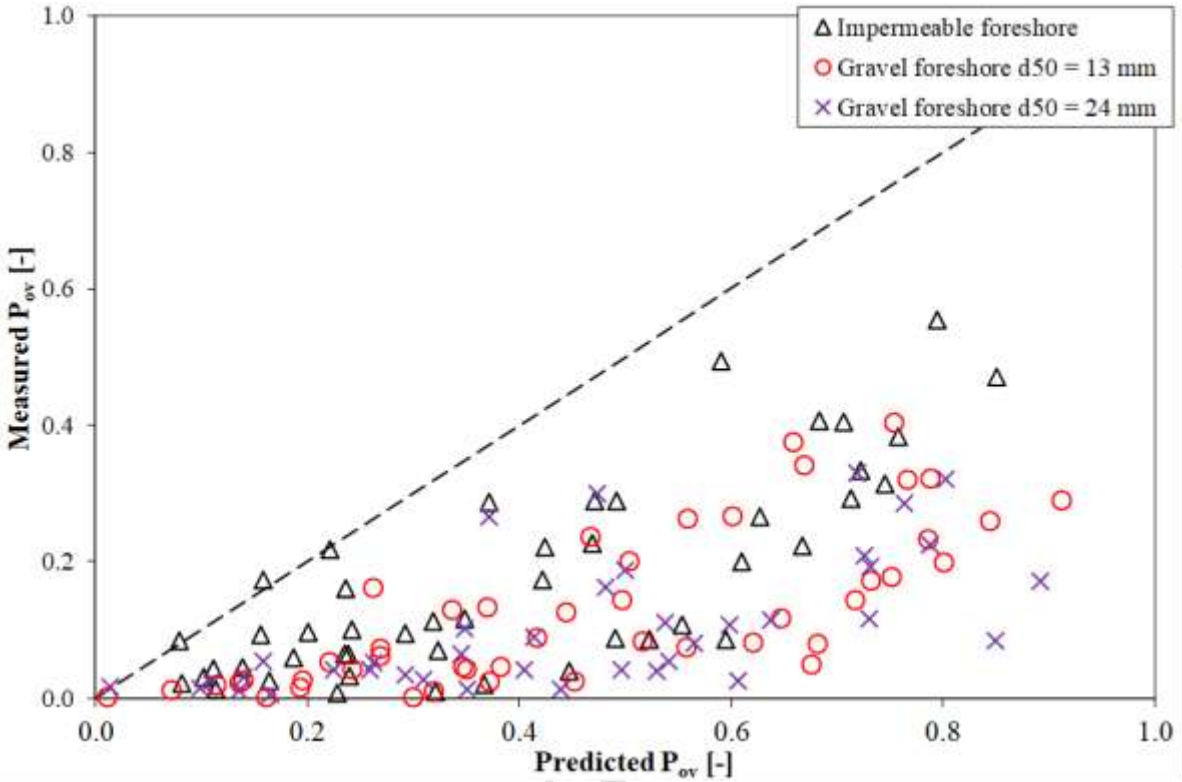

731 **Fig. 11.** A comparison of measured and predicted maximum overtopping volumes

732

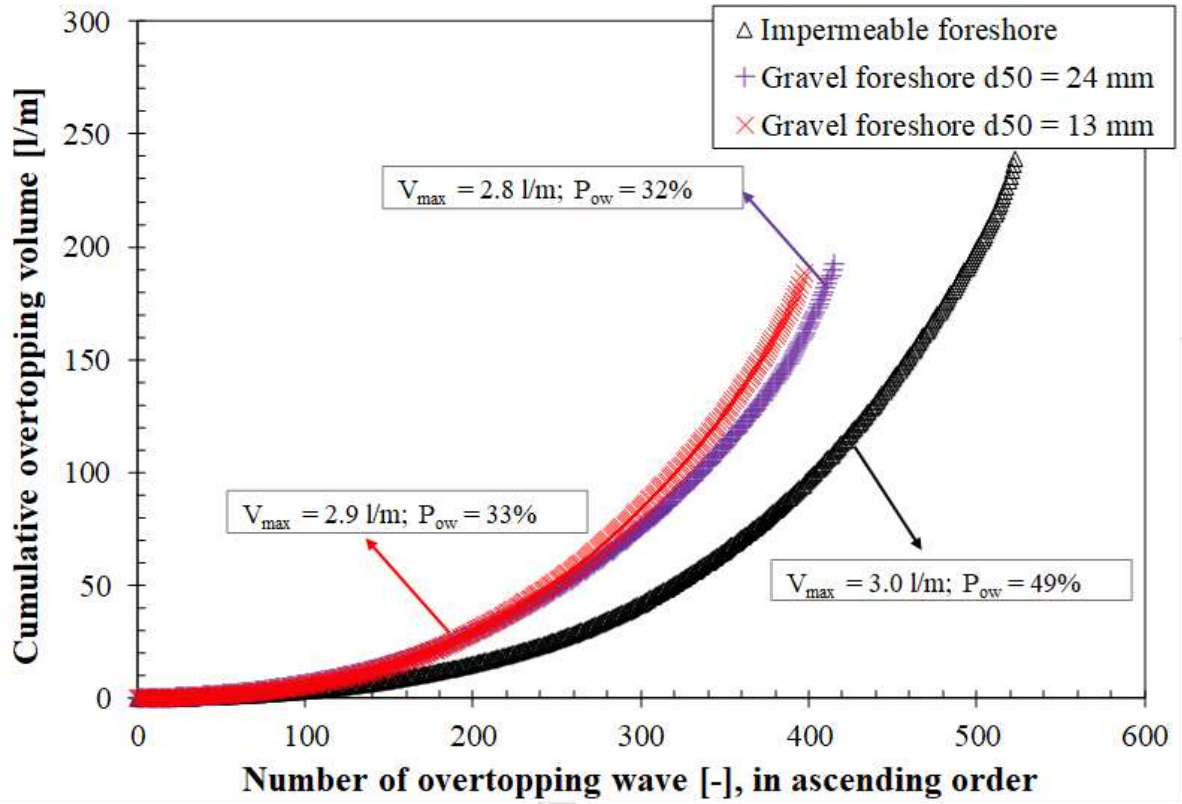

733 **Fig. 12.** Cumulative wave overtopping volumes against number of overtopping waves at sloping

734 structures with both impermeable and permeable foreshore configurations for

735 $s_{m-1,0}$ = 0.06, H_{m0} = 100 mm

736